Radiation Measurements 146 (2021) 106603

Contents lists available at ScienceDirect

Radiation Measurements

journal homepage: www.elsevier.com/locate/radmeas

Translation of the absorbed dose in the mobile phone to organ doses of an ICRP voxel phantom using MCNPX simulation of an Ir-192 point source

M. Discher [a,b,*], J. Eakins [c], C. Woda [a], R. Tanner [c]

[a] Helmholtz Zentrum München, Institute of Radiation Protection, 85764, Neuherberg, Germany
[b] Paris-Lodron-University of Salzburg, Department of Geography and Geology, 5020, Salzburg, Austria
[c] Public Health England, CRCE, Chilton, Didcot, Oxon, OX11 0RQ, United Kingdom

ARTICLE INFO

Keywords:
ICRP voxel Phantom
Mobile phone
Organ dose
Conversion factor
Retrospective dosimetry

ABSTRACT

Monte Carlo modelling has been performed to simulate aspects of the CATO exercise, which recreated the exposure of individuals on a bus to an Ir-192 point source. The modelling allowed a comparison and check of the measured data provided in (Rojas-Palma et al., 2020; Discher et al., 2021), and an investigation into the dose conversion coefficients that are required in order to use fortuitous dosemeters as indicators of absorbed doses to individuals; a conversion factor of 0.22 ± 0.01 was found to be appropriate to relate the phone dose to the average organ dose. The modelling also allowed some of the parameters of the experiment to be varied, and their impacts explored. In general, measured and modelled data agreed acceptably, with similar average doses and broadly similar variations in the results as a function of organ type.

1. Introduction

In the past decade there has been considerable interest in identifying and developing fortuitous personal dosemeters: items carried by the general population that may be used for individual dose reconstruction in the case of a radiological accident (Ainsbury et al., 2011). Some constituents of a mobile phone, like display glass (Discher and Woda, 2013) or electronic components on the circuit board, such as the aluminium oxide substrate of resistors (e.g. Inrig et al., 2008; Beerten et al., 2009; Ekendhal and Judus, 2012; Pascu et al., 2013), have been found to be sensitive to ionizing radiation, and have hence been considered as potential emergency dosemeters. Their dosimetric properties were subsequently tested and characterized by several laboratories using optically and/or thermally stimulated luminescence methods (OSL/TL). The usability and feasibility of these materials, and the dosimetry protocols that were developed to exploit them, have been demonstrated in several controlled inter-laboratory comparison exercises carried out within the EURADOS network (Bassinet et al., 2014; Fattibene et al., 2014).

With the aim of providing a field test of the use of mobile phones as emergency dosemeters, an exposure of a realistic irradiation scenario was performed at a military test site in 2014. This field test, named CATO (CBRN Architecture, Technologies and Operational procedures), served as a reconstruction of an accident that happened in Cochabamba, Bolivia, in 2002 involving an Ir-192 gamma source carried in the cargo hold of a bus, to which the passengers were exposed for the duration of their journey (IAEA, 2004). The reconstruction used anthropomorphic phantoms positioned in various seats of a bus to simulate the exposure of the individuals on-board. Mobile phones were placed on the phantoms in realistic locations. Routine physical dosimetry methods, such as electronic personal dosemeters (EPDs) and thermoluminescence dosemeters (TLDs), were also used on the anthropomorphic phantoms alongside the mobile phones: the results from these TLD and EPD measurements were compared against the dose assessments made using fortuitous dosemeters as a control (see details in Rojas-Palma et al., 2020 and Discher et al., 2021).

Despite the successes of the above, there exists a fundamental problem with the use of mobile phones as fortuitous dosemeters: the absorbed dose in the material of the fortuitous dosemeter represents a single measurement point that cannot automatically be associated with the transferred dose to the individual. Conversely, the desired endpoint of dose reconstruction is the absorbed dose in the body of the human, and not the absorbed dose in the mobile phone. Indeed, this problem may be common to fortuitous dosemeters in general, and contrasts strongly with the use of standard-issue dosemeters in routine radiological protection applications: the latter are designed and worn specifically

* Corresponding author. Paris-Lodron-University of Salzburg, Department of Geography and Geology, 5020, Salzburg, Austria.
E-mail address: michael.discher@sbg.ac.at (M. Discher).

https://doi.org/10.1016/j.radmeas.2021.106603
Received 27 January 2021; Received in revised form 21 May 2021; Accepted 25 May 2021
Available online 29 May 2021

to optimize the accuracy with which they can assess the personal dose equivalent to the individual. This tenet is not the case for fortuitous dosemeters, however, which could be located anywhere about the body and are neither tissue-equivalent nor originally intended to be used for dose measurements. As a consequence, in order for a fortuitous dosemeter to be of use in the triage process for medical treatment of those with high doses, it is necessary to correct the doses measured and convert them to the doses received by the individual.

The above correction may be achieved by performing radiation transport calculations to derive dose conversion factors that relate the measured dose in the fortuitous dosemeter to the dose to the individual (Van Hoey et al., 2021; Kim et al., 2019; Eakins and Ainsbury, 2018a,b). Eakins and Kouroukla (2015) performed such calculations for some generalized exposure scenarios, and investigated the effect of approximated locations of a mobile phone on a voxel phantom exposed in different geometries and to various source energies; their work was supported by measured data obtained using a Rando-Alderson phantom (Kouroukla, 2015). However, although conversion factors have been calculated for some general cases, they do not currently exist for all exposure scenarios, for example point sources located close to the body. Moreover, in the present case, the focus was on the dose to the display screen of the phone, rather than to the aluminium oxide substrate of resistors that was considered previously. There was hence a need to calculate new data that are relevant to the recent field-test reconstruction of the Cochabamba incident.

A joint research endeavour between EURADOS WG6 ('Computational dosimetry') and WG10 ('Retrospective dosimetry') addressed the question of how the absorbed dose measured in the fortuitous dosemeter can be linked to the absorbed doses to the organs in the body. The goal of the work was to perform a Monte Carlo simulation of the Cochabamba incident to derive dose conversion factors that are appropriate for the CATO reconstruction exercise. Similar to earlier work, the factors were determined using the combination of an anthropomorphic voxel phantom and a model of a mobile phone, to simulate the absorbed organ doses in the body and the absorbed dose in the fortuitous dosemeter, respectively. Using such calculated dose conversion factors, the absorbed dose in the mobile phone can be translated to appropriate dose quantities (organ doses) for the specific irradiation scenario. Moreover, the technique could be experimentally verified for a specific exposure scenario by comparing modelled and measured display glass dose results.

In addition to the wearing of routine and fortuitous dosemeters, the anthropomorphic phantoms of the CATO experiment also incorporated TLD elements throughout their volumes to estimate the dose distributions as a function of position in the body, and in turn assess the overall doses to its various organs. Together with the results for the mobile phones, these organ dose measurements are therefore supported by a second important use of the Monte Carlo simulations: to verify the experimental data by comparing modelled and measured results, and accordingly confirm the mapping of dose throughout the body. Confirmation of the measured data is important: although from one perspective TLD results might be considered reference data, as they are the most well-characterized, they still have significant limitations, such as the intrinsic TL-efficiency and non-tissue equivalence of their sensitive materials relative to the various organ materials, which are included correctly in the voxel models. Additionally, the modelling is beneficial in verifying the data from the phone experiments, which by their nature are inevitably less dosimetrically reliable. Overall, however, all of the measurements and models used within this CATO experiment are associated with significant uncertainties, so investigating agreements (or otherwise) across datasets provides essential insight into both endeavours. Moreover, the anthropomorphic phantom used for the measurements did not have limbs; the Monte Carlo modelling therefore also allowed an investigation into the likely impact of the absences of the arms and legs on the various organ doses within the body, giving insight into this potential limitation of the CATO approach.

2. Overview of materials and methods

The current section summarizes the measurements, noting that a fuller description is available in (Rojas-Palma et al., 2020; Discher et al., 2021). An overview of the general approach to modelling that was taken is also provided, noting that fuller details are provided in the subsequent section, where each modelling campaign is detailed along with the results that were obtained.

2.1. Simulation and calculation methods

The calculations were carried-out using the general-purpose Monte Carlo radiation transport code MCNPX (X-5 Monte Carlo Team, 2003; Shultis and Faw, 2011), which is widely used in radiation physics research for a variety of applications. The MCNPX model consisted of the ICRP 110 male voxel phantom (ICRP, 2009) as implemented at PHE (Jansen and Shrimpton, 2011) surrounded by an air-filled cylinder with a diameter of 50 m and a height of 4 m. The voxel phantom was combined with a model of a modern touchscreen mobile phone. The phone model included all of the major parts of the device, most of which were simplified as simple rectangular cells; the geometry and material specifications of the phone are detailed elsewhere (Discher et al., 2015). In order to replicate the experimental conditions of the CATO exercise, the mobile phone was fixed centrally on the front face of the voxel phantom at approximately the height of the pelvis. The phone was orientated such that its glass display screen faced away from the body and the entire display cell serves the detector.

Only photon transport was considered in the simulation (MCNP '*mode p*'), with the kerma approximation reasonably assumed. This improved the computational efficiency of the calculations, and hence statistical uncertainties on the results, and was justified on the grounds that secondary charged particle equilibrium would be anticipated in the real scenario: the materials of the phone, chair and surrounding air would likely provide sufficient build-up (ICRU, 1994) to the Ir-192 photons, which have a mean energy of ~0.3 MeV. Along with the dose absorbed by the glass screen of the phone, dose depositions were also tallied in a number of regions of interest within the body, including all organs identified as key to radiological protection by ICRP (ICRP, 2007). In general, these doses were recorded using photon track-length kerma tallies (MCNP '*f6:p*'). The exceptions to this were the doses to the red bone marrow (RBM) and endosteal tissue, which were estimated using fluence tallies (MCNP '*f4:p*') weighted by kerma factor multipliers (King et al., 1985; Cristy et al., 1987) in order to overcome problems associated with secondary charged particle inequilibria occurring on the scale of their microstructures. In addition to the doses to the various individual organs, and in accordance to the scheme adopted previously (Eakins and Kouroukla, 2015) the average dose to the whole body, D_B, was also assessed by simply averaging the absorbed doses to the 27 organs identified by ICRP 103 as being particularly radio-sensitive for stochastic effects and used in the definition of effective dose, without any additional weighting or processing.

2.2. Photon source and determination of the absorbed dose

The Ir-192 gamma source of the CATO reconstruction exercise was represented in the model by an ideal point source, with photons emitted isotropically with an energy distribution taken from a tabulated photon energy spectrum (Browne, 2003). The simplified form of the source is justified by its small dimensions, with the radioactive capsule having a diameter of only 2 mm. In principle, the encapsulation of a physical Ir-192 source would affect the energy spectrum, but precise information on this was not known at the time of modelling. In practice, however, the impact of this is likely to be low: any encapsulation would most strongly affect low-energy photons, but <8% of the fluence from the raw Ir-192 source has an energy <200 keV. The location of the source relative to the phantom was adjusted in accordance with the field experiment, and was

at a position that was 38 cm in front, 86 cm below, and 9 cm towards the right side (when viewed from face-on) relative to the approximate centre of the voxel phantom. The dose-per-source-particle tally results from the MCNP simulations were converted to absolute absorbed dose data using the decay-corrected activity of the source used in the CATO experiment (1.5 TBq), the exposure time (8 h), and the emission probability per decay (i.e. photon yield, $Y = 2.168$) for Ir-192 (Browne, 2003), allowing simulated and experimental results to be directly comparable to each other.

2.3. Experimental results from the anthropomorphic phantom

Equivalent doses in organs of the phantom were measured during the CATO experiment using many small thermoluminescence dosemeters (TLDs), which were placed throughout each slice of the phantom. MCP-N TLDs (LiF:Mg, Cu, P) calibrated in air and converted to dose (incl. energy dependence correction using the initial Ir-192 spectrum) in ICRU 40 tissue or bone were used to measure the equivalent organ doses in the phantom. Some parts of the phantom (e.g. legs, arms) were neglected and some organs (e.g. breast, heart, gall bladder and prostate) were not measured in the experiment. The absorbed dose in the mobile phone was measured using the "pre-bleached with blue LEDs" protocol (Discher and Woda, 2013). Full details of the experiment are available elsewhere (Rojas-Palma et al., 2020). The set-up used in the measurements is shown in Fig. 1.

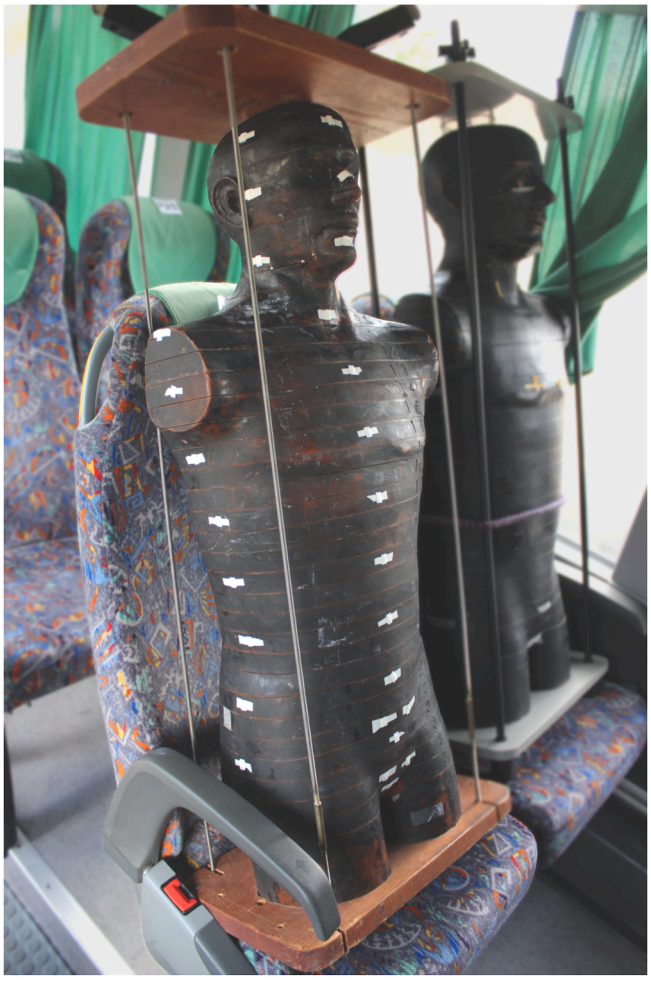

Fig. 1. The anthropomorphic phantom used in the CATO experiment. The phantom is equipped with thermoluminescence dosemeters (TLDs).

3. Models, results and discussion

In general, the statistical uncertainties on all of the MCNP results are of the order of ~1%; for clarity, they have therefore been omitted from the plots shown later. However, these values only reflect the variances within the inherently stochastic Monte Carlo process, and do not take into account the concurrent systematic or other uncertainties that might be associated with the modelling, which are much harder to quantify and are likely to be significantly greater. The uncertainties on the measured data are around 20%.

3.1. Modelled results of various exposure geometries

To confirm the initial set-up of the Monte Carlo model, the first step was to derive absorbed dose data for the organs when the phantom was exposed to Ir-192 from various exposure geometries: anterior-posterior (AP), posterior-anterior (PA), left-lateral (LLAT) and right-lateral (RLAT). The results of these simulations were then compared and cross-checked against the data given in Eakins and Kouroukla (2015), which were reported as the absorbed organ doses per fluence relative to the average organ dose, and were themselves benchmarked against data from ICRP Publication 116 (ICRP, 2010). The comparison showed good agreement between the two sets of calculated results: when like-for-like organ doses were compared, the average difference was only 0.1%, with the individual differences between the like-for-like organ doses distributed around this mean with a standard deviation of 1.5%. This cross-check indicated the correct compilation of the current model including the mobile phone and the unmodified voxel phantom model.

Next, the ICRP 110 adult male phantom was adapted in the simulation according to the exposure conditions of the Cochabamba incident (see Fig. 2). Specifically, the legs of the phantom were removed in order to provide a better representation of both an individual seated directly over a source and the limbless anthropomorphic phantom used in the CATO measurement (see Fig. 1). The environment surrounding the phantom was also modified by inserting a simplified model of a bus seat and a bus floor into the geometry, made of wood, PVC, aluminium and

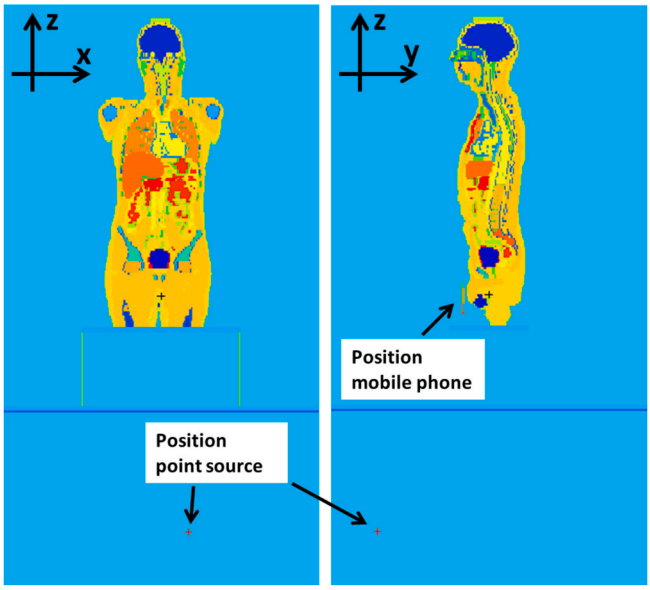

Fig. 2. Cross-sectional views in xz- (left) and yz- (right) planes through the ICRP Publication 110 adult male phantom used in the simulation, which was adapted to better match a seated individual; the bus seat and its floor were also included in the simulation. The mobile phone was fixed centrally on the front face of the phantom at the height of its pelvis (marked in the right-hand figure). The position of the point source relative to the phantom was adjusted in accordance with the field experiment and is marked in both views.

steel. This truncated model was used in the subsequent analysis of the dose to an individual on the bus, and hence for the determination of the conversion coefficient data presented later. In the real exposure, a second anthropomorphic phantom was located adjacently (Fig. 1), but this was not included in the simulations. The calculated results will therefore lack the small cross-scatter component to dose deposition, which would likely most impact those on the left side of the phantom, which is the side closest to where that second phantom would have been. Given the overall uncertainty budgets, however, the potential effects of this were assumed not to be noticeable during comparisons with measured data.

To test the suitability of the truncated geometry, the phantom was exposed to Ir-192 from AP, PA, LLAT and RLAT geometries. The results were then cross-checked against analogous data for the limbed phantom. The comparison showed a good agreement: there was an average difference of 0.7%, with individual differences between like-for-like organ doses distributed around this mean with a standard deviation of 2.2%. This demonstrates that the average organ doses are not greatly affected by the removal of the legs, as expected given that most organs are located deep within the body. However, the relatively small standard deviation does not highlight the few outliers.

3.2. Modelled results of point source

With the modelled set-up confirmed, the truncated phantom on its seat was exposed to the simulated Ir-192 point source. The absorbed doses to the organs that resulted from the calculation are shown in Fig. 3, along with the associated average organ dose and the dose to the phone glass. Also shown in Fig. 3 are the measured results obtained from the CATO experiment. The data are additionally summarized in the supplement.

In general, the results matched quite well: over a quarter of the simulation and experiment results are in agreement with each other to within 10%, whilst over half of the simulation and experiment results are in agreement with each other to within a few 10s of %. The two greatest discrepancies are for the lymph nodes and oral mucosa. This might be due to their small sizes and precise locations relative to many of the other organs, which may in turn perhaps have led to some of the largest uncertainties; these systematic variations would not be apparent just from the errors otherwise quoted here, which are only based on statistics for Monte Carlo and calibrations for measurements. Otherwise, there are no obvious strong correlations in the discrepancies between the experimental and modelled data. This might perhaps support the suggestion that the divergencies are caused more by inaccuracies in the measurements than in the Monte Carlo simulation: if instead there were a systematic fault in the geometry defined within the model, a stronger correlation with divergence and organ location might potentially have been expected. For example, the simulation was seen to over-estimate the measured dose to the stomach by more than it over-estimated the dose to the liver, even though those organs are located on the left and right sides of the body respectively, which indicates that the lack of cross-scatter in the model from the absent second phantom (Fig. 1) did not significantly impact the results.

The mean of all the simulated results (i.e. all organs and phone components) is 358 mGy, which is ~25% higher than the analogous mean experimental result (i.e. 287 mGy). Moreover, the measured and modelled average organ doses, D_B, as defined in Eakins and Kouroukla (2015), exhibited a similar difference, with the former 26.7% lower. If each dataset is normalized to its mean, then two thirds of the normalized simulated results agree with the normalized experimental results to within ±30%. This reinforces the observation that the distributions of doses within the measured and modelled datasets are broadly similar in shape, excluding a few outliers. However, a systematic difference clearly exists, with the simulated doses generally being higher than the measured ones; in fact, none may be resolved as being smaller when

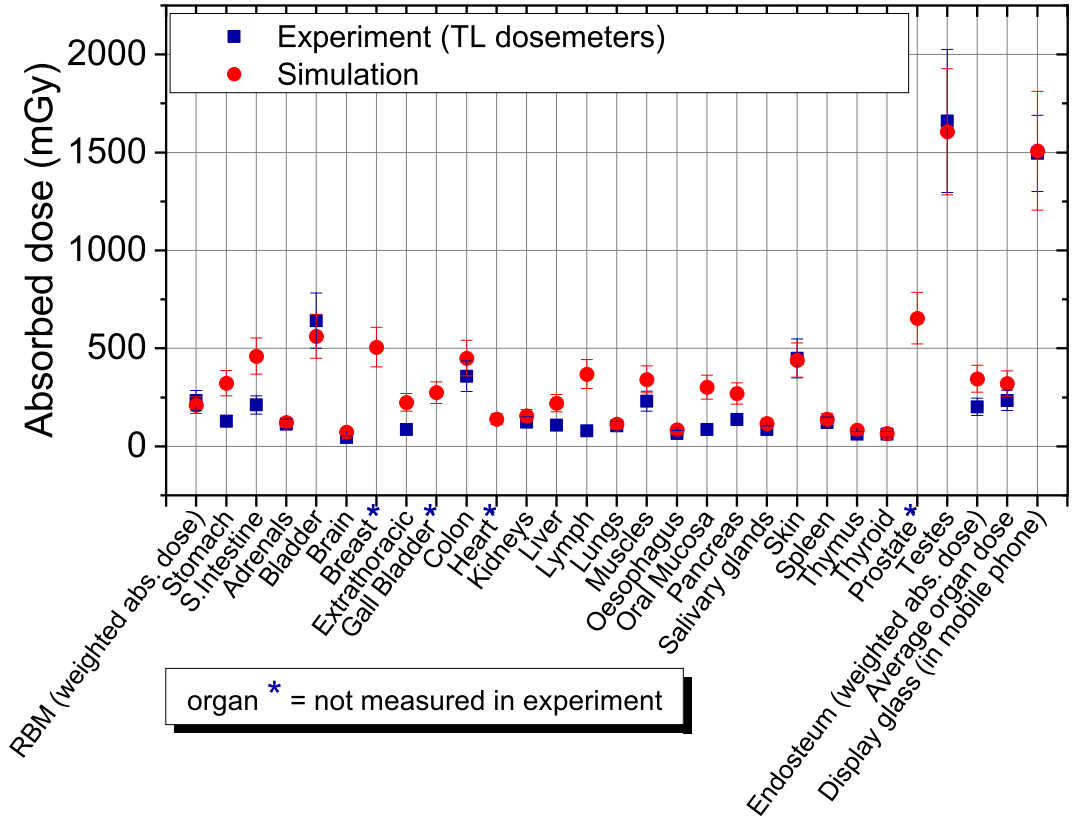

Fig. 3. Simulated dose results (red circles) in comparison with the experimental data (blue squares). (For interpretation of the references to colour in this figure legend, the reader is referred to the Web version of this article.)

uncertainties are taken into account. The exact cause of these discrepancy is not clear, but might suggest a source normalization issue, or the effects of not including sufficient shielding or encapsulation in the modelling. A further factor might be from missing shielding effects from other mobile phones that were used in the experiment but were not included in the simulation. Such systematic errors may be partially mitigable for practical dosimetry purposes, however, as discussed later. Nevertheless, given the many assumptions, approximations and uncertainties inherent in both the simulation and measurement campaigns, including the ~20% standard error quoted on the measured data, agreement in their results to within a few 10s of % may be considered a success, especially within the context of the limited degree of accuracy that is required for emergency dosimetry. Paraphrasing, given that calibration exposures may still be associated with quoted uncertainties of ~10% or so even when performed under the highly-controlled conditions of a metrology laboratory, anticipating agreement to within a few 10s of percent might be the best that could be hoped for in the results from irradiations performed as a field test, considering uncertainties resulting from factors such as ignorance of the precise positions of the phones and sources, the precise compositions of the phones and source (e.g. encapsulations), and the effects of surroundings and scatter etc. On the other hand, the measured and modelled display glass results agreed to 0.9%. This latter observation is arguably more important than the discrepancies found for the separate organs: the excellent agreement exhibited between the measured and modelled phone doses raises significant confidence in the reliability of this method of emergency dosimetry.

Simulated conversion factors from display glass doses to organ or average organ doses may be calculated by normalizing the data in Fig. 3 to the absorbed dose to the phone. These factors are presented in Fig. 4 and additionally in the supplement.

It is remarked that the derivation of conversion coefficients in this way potentially lessens the impacts of any systematic or absolute differences between modelled and measured datasets, at least for practical retrospective dosimetry purposes. Instead, interest here is mainly in relative relationships between one dose and another from within the same dataset, rather than from one of those datasets to the other. Specifically, because the process for obtaining coefficients entails dividing one simulated dose by another simulated dose, with that ratio then used to convert the measured doses, the existence of systematic differences between simulated and measured datasets will have less impact, because they may be partially cancelled when this quotient is taken.

In general, large differences in absorbed doses were found between mobile phone and body/organ doses, being up to a factor of more than 10 in some cases. Moreover, considerable variation across the dataset is apparent from Fig. 4. These observations are as expected from previous work (Eakins and Kouroukla, 2015), and are explainable by factors such as the location of the phone on the phantom, and the differing positions and depths of the organs within the phantom relative the point source, leading to differing levels of attenuation and shielding as a function of position, and hence differing dose depositions. Of course, these differences lead to the requirement for conversion coefficients to be generated and applied in order for the dosimetry system to be useful.

From the data of Fig. 4, a conversion factor of 0.22 ± 0.01 is seen to be appropriate to convert the absorbed dose measured in the phone glass to the concurrent average organ absorbed dose; the uncertainty quoted reflects just the statistical uncertainty from the Monte Carlo process, and not the systematic or other uncertainties arising from the conversion process (Eakins and Kouroukla, 2015). Thus, it is apparent that if the phone dose were assumed simply to equal the biological dose without this correction applied, the dose estimate for the individual would be over-estimated by a factor of nearly 5.

3.3. Uncertainty of the point source position

Repetitions of the simulations were carried out to investigate the effect of the source position on the modelled results. The position of the source was shifted ±10 cm in the *x*, y and *z* directions relative to its primary location, where *x* is the left-right, *y* is the front-back, and z is the vertical position of the source relative to the body (see Fig. 2). This is relevant because although the measurements were performed under nominally controlled conditions, the nature of the field test implied that those conditions were known only approximately (in comparison to the

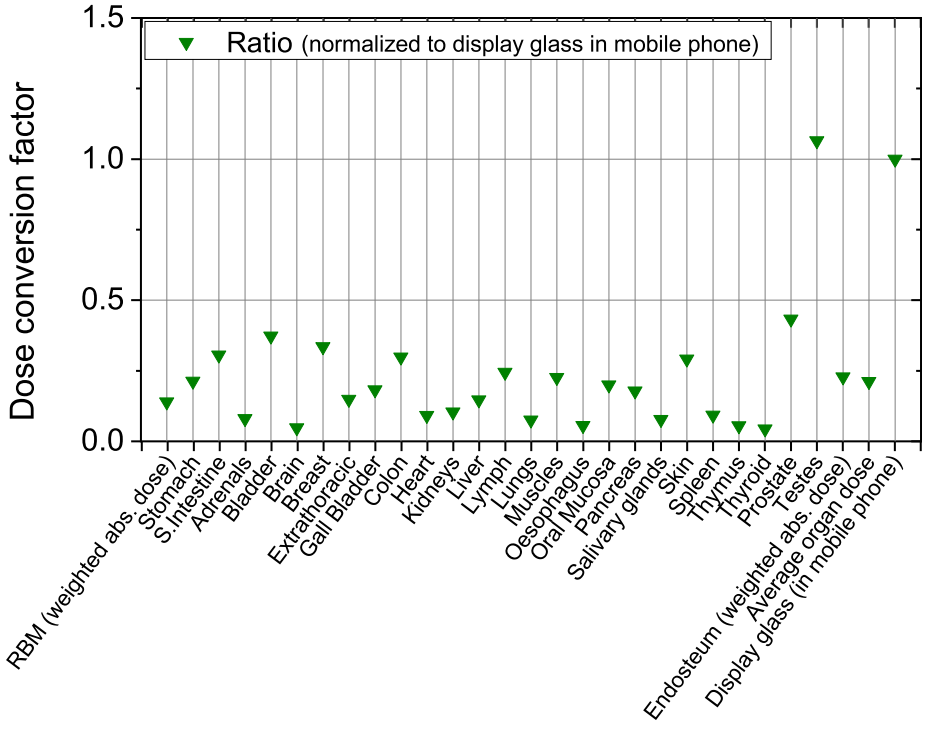

Fig. 4. Simulated conversion factors calculated by normalizing the organ and average organ data to the dose in the mobile phone.

'proper' calibration conditions typically enforced by metrology laboratories, for example), so factors such as the precise location of the source relative to the phantom may be known only with limited accuracy. The perturbations of ±10 cm therefore serve to provide a handle on the maximum plausible uncertainty from this ignorance.

For each perturbation of the source position, ratios were calculated of each new organ dose relative to that obtained when the source was at its original location; the average of these ratios was then calculated. The standard deviation in the set of ratios around this mean was also calculated, to demonstrate the magnitude of the induced divergences in the results for the individual organs. The results from the systematic variations of the source are shown in Table 1.

Changes of ±10 cm in the x direction did not significantly affect most of the modelled results, due to the symmetries of most organs within the body about its left-right axis. The most affected organ in Table 1 was the stomach, as expected due to the asymmetric location of that organ about the body's centre line. However, changes in the *y* and *z* direction had a bigger impact on the averages of the organ doses: a shift of the source position of just ±10 cm can lead to changes of more than 20% in the results. Moreover, relocations in the *y* direction also caused large variations in the magnitudes of the changes to the individual organ doses, as seen from the larger standard deviations of those two datasets. These observations are explainable primarily by the inverse-square divergence of the isotropic point-source, but also by additional factors such as differing shielding contributions from different parts of the body as the source is moved relative to it. For example, moving the source further from the body in the negative y direction increases inverse square separation from the brain, but also increases the line-of-sight solid angle between that organ and the source. There is therefore less attenuation of the field, and hence an enhanced dose. For the z shift, generally, organ doses vary in the expected way with movement in the height of the source: those organ doses closest to the source (e.g. kidneys, small intestine) are most affected, whilst those further away (e.g. brain) are less impacted. This is as anticipated, with a 10 cm shift representing a greater fractional change in distance at smaller separations, and hence proportionally greater impact from inverse square.

It is possible that the results of Table 1 might help to explain one of the trends exhibited in the data of Fig. 3. In particular, it was observed that almost all of the modelled organ doses were higher than their corresponding measured doses, with an average difference of ~30%. These systematic differences could be due to uncertainty on the precise location of the source in the experiment: if the source in the CATO experiment was actually positioned slightly lower than has been assumed in the model, for example, the impact on the results could be similar to that exhibited in Fig. 3. Uncertainties in the *y* and *z* locations could easily generate the systematic differences between modelling and measurement that have been observed. Note that the above explanation might also imply that similar source location effects should be observed between the calculated and measured doses to the glass screen. However, whilst these might have occurred, they are not possible to resolve within the uncertainties on the results: the 20% variation from the 10 cm displacements is comparable to the 20% error bars on the TL measurement of the phone. Generalizing these observations, it is suggested that when determining and then applying phone to organ dose conversion coefficients for isotropic point sources, the precise location of the source may be critical to the results that are obtained.

Of course, other factors will also be very important, such as the precise location of the phone. The impacts of large differences in phone location have been considered elsewhere (Eakins and Kouroukla, 2015), which provided exploratory investigations of this parameter: four phone positions about the body and seven exposure geometries were systematically simulated and investigated, and conversion coefficient data produced. However, the actual values of the conversion coefficients will also be impacted by the effects of smaller differences, such as small perturbations about those 'reference' conditions, for example for a phone displaced by a few centimetres in some direction or from ignorance of its exact location in a real exposure. Again, this emphasizes the value of endeavours such as the CATO experiment and the current simulations, with the measurements and modelling seen to complement each other: a comparison of their nominally identical but practically different set-ups leads to results that help to inform the uncertainty budget for retrospective dosimetry in realistic and non-standard exposure conditions.

3.4. The effect of arms on the anthropomorphic phantom

As a final test, an additional geometry was defined in which the arms of the phantom were removed as well as the legs, thereby providing a better match to the anthropomorphic phantom actually used in the CATO reconstruction experiment. This limbless phantom was then exposed to the Ir-192 point source located at the same position as before. The results of the simulation were then compared against the data derived previously for the legless phantom (Fig. 3). The comparison showed good agreement between the calculated results for the two phantoms: the pairs of datasets exhibited an average difference of only 4.1%, with the individual differences between like-for-like organ doses distributed around this mean with a standard deviation of 4.2%. However, although like-for-like organ doses generally agreed to better than 14%, doses in the limbless phantom were consistently lower, perhaps due to the lack of cross-scatter of photons into the target regions by the arms. Nevertheless, this comparison demonstrates that although for some organs the impact may be sizeable, overall the organ doses are unlikely to have been greatly affected by the removal of the arms in the CATO reconstruction, as expected given the position of the source below the body. Moreover, in both cases the calculated dose absorbed by the mobile phone was the same, leading to a phone to average organ dose conversion factor for the limbless phantom that was only a few per cent lower than that for the truncated phantom with arms.

Table 1
Average ratios between simulated organ doses for different locations of the point source relative to its primary position. Differences for selected organs are additionally shown.

New position	Average ratio	Standard deviation around mean ratio	Selected organ dose ratios to primary source location							
			RBM (weighted absorbed dose)	Stomach	S.Intestine	Brain	Heart	Kidneys	Lungs	Skin
x minus 10 cm	1.00	0.04	1.00	0.94	1.00	1.02	0.98	0.98	0.96	1.01
x plus 10 cm	0.99	0.05	1.00	1.01	0.99	1.00	1.05	0.97	1.05	0.97
y minus 10 cm	1.16	0.23	1.09	1.08	1.10	1.35	1.18	1.21	1.19	0.98
y plus 10 cm	0.81	0.12	0.91	0.82	0.78	0.64	0.78	0.73	0.76	0.99
z minus 10 cm	0.82	0.03	0.82	0.81	0.79	0.84	0.82	0.77	0.83	0.84
z plus 10 cm	1.24	0.04	1.26	1.21	1.27	1.22	1.23	1.29	1.21	1.21

4. Summary and conclusions

Monte Carlo modelling has been performed to simulate the CATO exercise, which recreated the exposure of individuals on a bus to an Ir-192 point source. The modelling allowed a comparison and check of the measured data, and an investigation into the dose conversion coefficients that are required to use fortuitous dosemeters as indicators of absorbed doses to individuals. Moreover, the modelling allowed some of the parameters of the experiment to be varied, and their impacts explored. For example, the results were found (Table 1) to depend on the position of the point source relative to the individual: even small relocations (±10 cm) of the Ir-192 led to significant variations in the doses. This observation is important, because it implies that the precise location of the point source will be critical to the values of any phone to organ dose conversion coefficients that are calculated. In general, however, measured and modelled data agreed acceptably (Fig. 3), with similar average doses and similar variations in the results as a function of organ type.

One potential limitation of the anthropomorphic phantom used in the CATO exercise was the absence of limbs. In response to this, the Monte Carlo model was used to investigate the impact of the limbs on the resulting organ doses. The cross-scatter of photons by the limbs was seen to contribute small but significant components of absorbed dose to the visceral organs, which will be absent in the CATO measurements and hence impact upon the results reported from it (Rojas-Palma et al., 2020).

In principle, the conversion factor data shown in Fig. 4 could be used to translate the absorbed dose in the mobile phone into the individual organ doses and/or associated average organ dose for the simulated exposure scenario. In this case, a factor of 0.22 ± 0.01 should be applied to the measured dose to reconstruct the whole body dose to the individual. Indeed, this conversion process is vital in retrospective dosimetry in order for the measured physical dose to be related to the biological dose, as required for medical triage.

During a real radiological emergency, the choice of conversion coefficient to apply would be specific to the precise exposure conditions that exist for each individual, also taking into account other factors such as the location of the phone relative to them. Ideally, then, the optimum approach under such circumstances would be to repeat the type of process described in this paper, with realistic models created that faithfully replicate the specific geometries of interest and that can be run to generate bespoke conversion data on a case-by-case basis. In practice, however, such an approach would be feasible only in a very small-scale incident, in which only very few individuals were exposed. Moreover, even then the results would likely only find application in subsequent 'forensic' analyses, with a lack of available resources and complexity in producing the data inevitably preventing their generation in time for earlier triage purposes (Eakins and Ainsbury, 2018a, 2018b). In a larger scale event, therefore, generic conversion data would need to be applied, which are less accurate but may be pre-calculated and tabulated in advance. This need reinforces the usefulness of studies such as the current one in contributing to understanding of overall uncertainty budgets, which are shown to be relatively large (~few 10s of percent) even when the geometry is comparatively well-known and the exposure well-controlled. A larger study into generic versus bespoke conversion coefficient data, and their impact on dose uncertainty within a practical exposure scenario (Waldner et al., 2021), is currently an active area of research within EURADOS WG10.

Declaration of competing interest

The authors declare that they have no known competing financial interests or personal relationships that could have appeared to influence the work reported in this paper.

Acknowledgements

The authors want to thank Jan Jansen (PHE) for providing the voxel phantom code in MCNPX format, and Jérémie Dabin (SCK-CEN) for providing the experimental results (TL dosemeters) of the anthropomorphic phantom in the CATO field experiment. The visit of Michael Discher to Public Health England was gratefully supported by the EURADOS e.V. Research Grant (2014).

Appendix A. Supplementary data

Supplementary data to this article can be found online at https://doi.org/10.1016/j.radmeas.2021.106603.

References

Ainsbury, E.A., et al., 2011. Review of retrospective dosimetry techniques for external ionising radiation exposures. Radiat. Protect. Dosim. 147, 573–592.
Bassinet, C., et al., 2014. Retrospective radiation dosimetry using OSL of electronic components: results of an inter-laboratory comparison. Radiat. Meas. 71, 475–479.
Beerten, K., Woda, C., Vanhavere, F., 2009. Thermoluminescence dosimetry of electronic components from personal objects. Radiat. Meas. 44, 620–625.
Browne, E., 2003. NM - CEA/LNHB - table de Radionucléides, laboratoire national henri becquerel. Available from: http://www.nucleide.org/DDEP_WG/Nuclides/Ir-192_tables.pdf. (Accessed 28 September 2019).
Cristy, M., Eckerman, K.F., 1987. Specific Absorbed Fractions of Energy at Various Ages from Internal Photon Sources. ORNL Report: ORNL/TM-8381/vol. 1.
Discher, M., Woda, C., 2013. Thermoluminescence of glass display from mobile phones for retrospective and accident dosimetry. Radiat. Meas. 53–54, 12–21.
Discher, M., Hiller, M., Woda, C., 2015. MCNP simulations of a glass display used in a mobile phone as an accident dosimeter. Radiat. Meas. 75, 21–28.
Discher, M., Woda, C., Ekendahl, D., Rojas-Palma, C., Steinhäusler, F., 2021. Evaluation of physical retrospective dosimetry methods in a realistic accident scenario: results of the CATO field test. Radiat. Meas. 142, 106544.
Eakins, J.S., Kouroukla, E., 2015. Luminescence-based retrospective dosimetry using Al_2O_3 from mobile phones: a simulation approach to determine the effects of position. J. Radiol. Prot. 35, 343–381.
Eakins, J.S., Ainsbury, E.A., 2018a. Quantities for assessing high doses to the body: a short review of the current status. J. Radiol. Prot. 38, 731–742.
Eakins, J.S., Ainsbury, E.A., 2018b. Quantities for assessing high photon doses to the body: a calculational approach. J. Radiol. Prot. 38, 743–762.
Ekendhal, D., Judas, L., 2012. Retrospective dosimetry with alumina substrate from electronic components. Radiat. Protect. Dosim. 150, 134–141.
Fattibene, P., et al., 2014. EPR dosimetry intercomparison using smart phone touch screen glass. Radiat. Environ. Biophys. 53, 311–320.
IAEA - International Atomic Energy Agency, 2004. The Radiological Accident in Cochabamba, ISBN 92-0-107604-5. Vienna.
ICRP - International Commission on Radiological Protection, 2007. The 2007 recommendations of the International Commission on radiological protection. ICRP Publication 103 ann. ICRP 37 (2–4).
ICRP - International Commission on Radiological Protection, 2009. Adult reference computational phantoms. ICRP Publication 110. Ann. ICRP 39 (2), 1–165.
ICRP - International Commission on Radiological Protection, 2010. Conversion coefficients for radiological protection quantities for external radiation exposures. ICRP (Int. Comm. Radiol. Prot.) Publ. 116.
ICRU - International Commission on Radiation Units and Measurements, 1994. Stopping Powers for electrons and positions. ICRU (Int. Comm. Radiat. Units Meas.) Rep. 37.
Inrig, E.L., Godfrey-Smith, D.I., Khanna, S., 2008. Optically stimulated luminescence of electronic components for forensic, retrospective and accident dosimetry. Radiat. Meas. 44, 726–730.
Jansen, J.T.M., Shrimpton, C., 2011. Calculation of normalised organ and effective doses to adult reference computational phantoms from contemporary computed tomography scanners. Prog. Nucl. Sci. Technol. 2, 165–171.
Kim, M.C., Kim, H., Han, H., Lee, J., Lee, S.K., Chang, I., Kim, J.-L., Kim, C.H., 2019. A study on dose conversion from a material to human body using mesh phantom for retrospective dosimetry. Radiat. Meas. 126, 106126.
King, S.D., Spiers, F.W., 1985. Photoelectron enhancement of the absorbed dose from X-rays to human bone marrow: experimental and theoretical studies. Br. J. Radiol. 58, 345–356.
Kouroukla, E., 2015. Luminescence Dosimetry with Ceramic Materials for Application to Radiological Emergencies and Other Incidents. Doctoral thesis. Durham University.
Pascu, A., Vasiliniuc, S., Zeciu-Dolha, M., Timar-Gabor, A., 2013. The potential of luminescence signals from electronic components for accident dosimetry. Radiat. Meas. 56, 384–388.
Rojas-Palma, C., Woda, C., Discher, M., Steinhäusler, F., 2020. On the use of retrospective dosimetry to assist in the radiological triage of mass casualties exposed to ionizing radiation. J. Radiol. Prot. 40, 1286–1298.
Shultis, J.K., Faw, R.E., 2011. An MCNP primer. Available from: http://www.nucleonica.net/wiki/images/6/6b/MCNPprimer.pdf. (Accessed 10 September 2016).
Van Hoey, O., Römkens, D., Eakins, J., Kouroukla, E., Discher, M., Vanhavere, F., 2021. Uncertainty evaluation for organ dose assessment with optically stimulated

luminescence measurements on mobile phone resistors after a radiological incident. Radiat. Meas. 141, 106520.

Waldner, L., Bernhardsson, C., Woda, C., Trompier, F., Van Hoey, O., Kulka, U., Oestreicher, U., Bassinet, C., Rääf, C., Discher, M., Endesfelder, D., Eakins, J., Gregoire, E., Wojcik, A., Ristic, Y., Kim, H., Lee, J., Yu, H., Kim, M.C., Abend, M., Ainsbury, E., 2021. The 2019-2020 EURADOS WG10 and RENEB field test of retrospective dosimetry methods in a small-scale incident involving ionizing radiation. Radiat. Res. 195 (3), 253–264. https://doi.org/10.1667/RADE-20-00243.1}.

X-5 Monte Carlo Team, 2003. MCNP: A General Monte Carlo N-Particle Transport Code, Version 5, Vol. II. User's Guide, Los Alamos National Laboratory Report LACP-03-0245.